IEEE Access
Multidisciplinary | Rapid Review | Open Access Journal

Received November 29, 2017, accepted December 26, 2017, date of publication January 23, 2018,
date of current version March 13, 2018.

Digital Object Identifier 10.1109/ACCESS.2018.2796939

Hybrid Electric Powertrain Design Methodology With Planetary Gear Sets for Performance and Fuel Economy

OGUZ H. DAGCI[1], HUEI PENG[2], and JESSY W. GRIZZLE[1], (Fellow, IEEE)
[1]Department of Electrical Engineering and Computer Science, University of Michigan, Ann Arbor, MI 48109, USA
[2]Department of Mechanical Engineering, University of Michigan, Ann Arbor, MI 48109, USA

Corresponding author: Oguz H. Dagci (oguzhada@umich.edu)

ABSTRACT Planetary gear sets (PGs) play a key role in the design of hybrid electric vehicles (HEVs) because they allow the realization of many unique powertrain designs using a limited number of components. By leveraging the capability of this mechanical device, an automated design process for PG-based HEV systems focusing on both fuel economy and performance is introduced in this paper. The design process consists of five major stages. In the first stage, all possible powertrain modes of an HEV design are automatically generated with a given set of powertrain components. In the second stage, all powertrain types that can be formed with a given set of components are mathematically identified, and each feasible mode is classified under one of these powertrain types. In the third stage, computationally efficient linear programming solvers suitable for vector operations are developed for each powertrain type to assess the gradeability, launch torque, overtaking torque, and acceleration time of each mode for all PG gear ratio combinations. In the fourth stage, the combination of modes that meets the performance requirements, and the number and location of clutches that make these mode transitions possible, are explored. As a result, each potent mode combination, the clutches necessary for the mode transition, and the auxiliary modes established as a result of all clutch state combinations constitute a design that meets the performance criteria. In the last stage, the fuel economy improvement potential of each competent design is evaluated. The results show that light-duty truck performance requirements can be met by many two-PG HEV designs without sacrificing fuel economy if the appropriate analysis and synthesis techniques for exploring the entire design space are developed.

INDEX TERMS Exhaustive search, fuel economy, hybrid electric vehicles, hybrid electric vehicle design process, optimal design, performance, planetary gear set, powertrain design.

I. INTRODUCTION

In the automotive industry, three pillars of competition are fuel economy, performance, and safety. Since fuel economy and safety standards have been already set to high levels by regulators [1], [2], little room for competition remains in these areas. As these standards go into effect, performance would likely be the key pillar where automotive companies can make a difference. The situation becomes even more critical in the U.S., given the sheer market share of light-duty trucks and sport-utility vehicles with high performance requirements [3], [4]. Companies that can offer products with high fuel economy and superior performance will meet both the requirements of the regulators and the expectations of the customers. Thus, in recent years, hybrid electric vehicles (HEVs) have become a cost effective solution for overcoming these issues [5]–[8].

When HEV products in the U.S. market are analyzed, the success of HEVs designed with planetary gear sets (PGs) is undeniable, as 85% of HEVs sold in the U.S. market use PGs in their powertrain system [9]. The reason for this success comes from the simplicity and design flexibility of PGs. Although PGs have simple governing equations, the huge number of combinations that can be realized with PGs and powertrain components such as engine, electric machines, and clutches gives engineers an opportunity to optimize the powertrain for both fuel economy and performance. In this paper, how to take advantage of this large design space will be shown by deriving the necessary design analysis and

synthesis methods, and by introducing a systematic design process.

If we are to exploit the full potential of PGs in an HEV design, all candidates in the design space must be explored, which means that:

1) Design candidates should be evaluated against both fuel economy and performance criteria (gradeability, launch torque, overtaking torque, acceleration time between various speed intervals, top speed, backward driving capability) used in a full-fledged HEV powertrain design.
2) The design candidates that can be generated with a given set of components should be manageable in size.
3) The design synthesis methods should be able to perform component sizing analyses.
4) No single HEV powertrain type should be excluded from the process.

Although several HEV design methodologies have been introduced in the past 10 years [10]–[19], they fall short in meeting all of these requirements. In the first attempt to introduce PG-based hybrid electric powertrain design methodology, the number of PGs, clutches, brakes, and electric machines are initially determined, and then all possible kinematic combinations of these elements are analyzed using graph theory and algebraic design techniques [10]. Vehicle performance and fuel economy, however, are not taken into account in that work. This gap is partially filled in [11] by taking 0-50mph time and the potential for fuel economy improvement of candidate designs into account. The drawbacks of that study are the inclusion of only power-split type in the design process, and the assumption of constant vehicle power during the evaluation of 0-50mph time. Zhang *et al.* [13], [16] improve the process in [11] by developing an automatic modeling and screening process that conducts an exhaustive search of all designs with different configurations, clutch locations, operating modes, and powertrain types. The method for generating the design space is based, however, on evaluating all possible configurations, which grow to an unmanageable number if the variation of component sizes is taken into account. Furthermore, its method for deriving speed and torque relationships is not suitable for PG gear ratio variation.

A new design approach called mode-based design is adopted in [13] and [16] by slightly modifying the work of [13], [16]. Since this work uses the same automatic modeling and screening process in [13], [16], it possesses all the same drawbacks. Another disadvantage of the mode-based design in [19] is to categorize the feasible modes as fuel saving or high performance modes, although a mode's behavior can change with respect to driving conditions such as vehicle speed and vehicle load.

In contrast to the exhaustive design approaches in these studies, a generalized representation of a power-split configuration with two PGs is proposed by [12]. In this approach, the designs that meet the design requirements are generated by the proper selection of gear ratios in the generalized power-split configuration. However, this method is solely applicable to power-split powertrain types and is not capable of generating unique multi-mode designs. Bayrak *et al.* [17] improve this concept by using genetic algorithms and sequential quadratic programming to identify kinematic relationships of superior power-split or full-electric single or two-mode designs. However, this approach requires a large number of initial population and does not guarantee convergence to an optimal design. Moreover, since a description of performance evaluation is missing from the paper, an over-simplified performance analysis is to be expected.

In contrast to all of these complete design frameworks, the study in [15] proposes only an automatic topology generator based on constraint logic programming without taking into account the component sizes, fuel economy, and performance. Hence, this work is not able to generate practical designs.

The first study where an accurate performance analysis is conducted in addition to a fuel economy evaluation implements an instantaneous optimization algorithm for full-load analysis [14]. The proposed method evaluates all torque and speed combinations of all components in a design candidate at each simulation step during a 0-60mph time calculation. Hence, the computational load of this method is heavy, and only a small design space can be handled in practice. As a result, this approach can be applied solely to power-split powertrain types with a single PG.

This paper introduces a novel design framework that overcomes the deficiencies from previous studies. It not only assesses all design candidates in terms of both complete performance criteria and fuel economy but also includes all feasible powertrain types in the design space. Though based on an exhaustive search, thanks to the mode-based design approach, the design space is manageable in size. The proposed method of deriving the characteristics equations of the modes facilitates computationally efficient component-sizing exercises, including variation in PG gear ratios. Once the infeasible modes are eliminated from the design space, rigorous performance evaluations, which rely on newly developed linear programming solvers, are conducted to eliminate as many modes as possible in the early design stage. Two modes that can transition to each other via a maximum of three clutches and can meet collectively all performance criteria are identified as high performance mode pairs. Each potent mode pair, with the auxiliary modes that are formed through all clutch state combinations, constitutes a design candidate, which then goes through fuel economy evaluation. The fuel economy simulation results reveal that many high performance and fuel efficient designs are realizable with just two PGs if a process with strategically selected design steps and synthesis/analysis tools is in place.

The paper is organized as follows. Sections II and III explain how the design space is generated and what the proposed design process is. In Sections IV and V, an automated modeling procedure and a mode screening and powertrain type identification process are introduced.

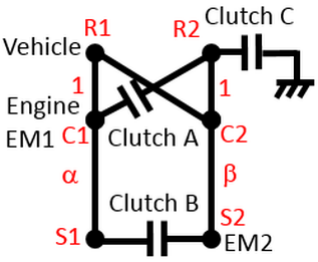

FIGURE 1. Configuration example.

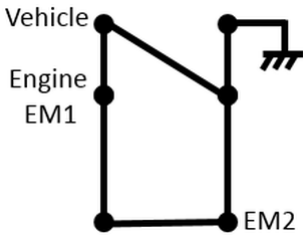

FIGURE 2. Mode example.

Sections VI and VII describe the methods that efficiently evaluate the modes with respect to PG gear variations and forward/backward speed capability. The performance criteria and related analysis and synthesis algorithms are explained in Section VIII. Sections IX-XIII show the steps that create the competent designs by combining the appropriate modes. Section XIV presents fuel economy simulations and the best designs in terms of performance and fuel economy.

II. GENERATION OF DESIGN SPACE

Before describing the steps of the proposed design framework, we must first determine what elements make up the design space. Three elements are possible: component-, configuration- and mode-based elements. In the component-based case, the design elements are the components that may be used in a hybrid transmission (e.g., engine, electric machines, planetary gearbox, differential, clutches). The disadvantage of this approach is that it results in an extremely large design space due to the fine granularity. Component-based design space is used only in [15] with an incomplete design process, where component sizes, fuel economy, and performance are not taken into account. The more realistic approaches are configuration- and mode-based designs, where the design elements are at a coarser granularity. In the configuration-based design, predefined components including clutches are assigned to the PG nodes. Each combination is named as one configuration and is a complete hybrid transmission design in and of itself. Fig. 1 shows a configuration example, where each PG is represented as a lever with three nodes, each of which corresponds to ring (R), carrier (C) and sun (S) gears of the PG. The lengths between ring-carrier nodes and carrier-sun nodes on the lever are taken as 1 and N_R/N_S, where N_R and N_S are the tooth numbers of ring and sun gears. In this paper, θ_1 and θ_2 represent N_R/N_S of two PGs, respectively. In contrast to a configuration, a mode is generated by assigning predefined components, apart from clutches, to the PG nodes. A mode corresponds to the dynamics for a given state of the clutches in a configuration. Fig. 2 shows one mode of the configuration in Fig. 1, where Clutches B and C are closed, while Clutch A is open. In the mode-based design approach, once all modes are generated in the design space, the groups of modes that collectively meet the design specifications are then identified. If the modes in a group can transition to each other with the predetermined number of clutches, this mode group constitutes a valid design and is evaluated for other criteria, such as fuel economy. In this study, the mode-based design approach is chosen. Since mode-based design and its advantages over other approaches have not been explored sufficiently well in the literature, the rationale behind this decision follows.

1) Design space in the mode-based design is much smaller than in the other approaches. In this study, the designs that can be generated with two PGs, one engine, two electric machines, one vehicle output shaft, and at most three clutches are investigated. The reason of choosing two PGs is the size of generated design space. With one PG, the maximum number of modes is 54, whereas the number of modes in two-PG case is 49,824, which provide much bigger and flexible design space for exploration. Furthermore, the maximum number of clutches is set to three with the assumption of the existence of competent designs with three clutches that can meet all design requirements.
   For the configuration-based design, at most three clutches can be assigned to the PG nodes, as $C_{15}^3 + C_{15}^2 + C_{15}^1 = 575$ different ways. If we constrain the engine and vehicle output to not be on the same PG node, all components can be assigned to six PG nodes as $6 \times 5 \times 6 \times 6 = 1,080$ ways. The design space for the configuration-based approach becomes $621,000$. In the mode-based design approach, the modes can be grouped according to the number of connections between two PGs. For one, two, and three connections between two PGs, we can generate 9, 36, and 44 different connections, respectively. The components can be assigned to the PG nodes for these three types of connections $5 \times 4 \times 5 \times 5 \times 2^3 = 4,000$, $4 \times 3 \times 4 \times 4 \times 2^2 = 768$, and $3 \times 2 \times 3 \times 3 \times 2^1 = 108$ ways. 2^x terms in these calculations come from the possibility of assigning a brake to the PG nodes without an engine or vehicle. Based on these results, the design space for the mode-based approach becomes $68,832$, which is almost ten times smaller than the configuration-based design space. When another design variable such as the PG gear ratio is introduced to the design problem, the design space grows even further, and the advantage of a mode-based design becomes more apparent.
2) In the configuration-based design, the assignments of the components to the PG nodes are fixed in a

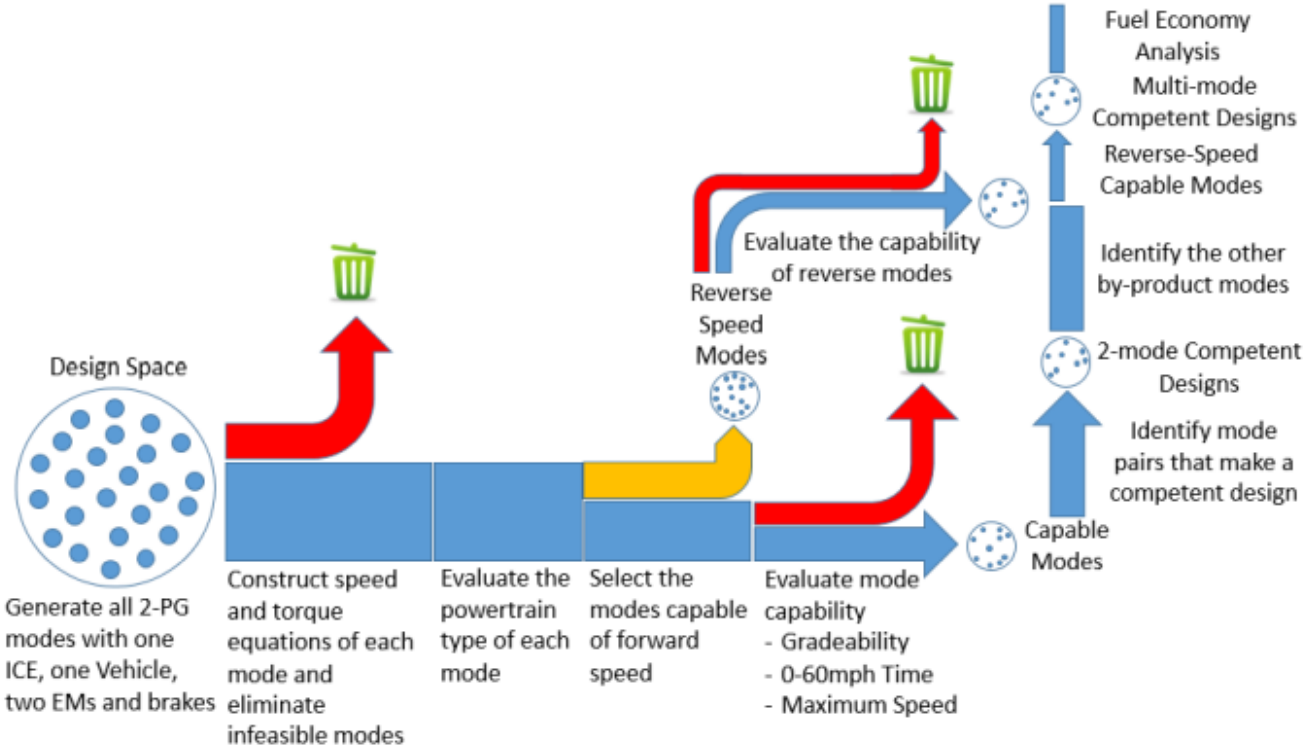

FIGURE 3. Proposed design process.

design candidate. In the mode-based design, this constraint does not exist, and the PG node assignment of a component can be different in any two modes of a design.

3) The mode-based design is computationally efficient compared to the configuration-based design because a unique mode exists in multiple configurations and is evaluated multiple times in a configuration-based design.
4) Configuration-based design should limit the number of clutches in a design due to the large number of design candidates. Because mode-based design applies the constraint of clutch number at the last stage, any two modes can be in a design as long as they provide superior performance and fuel economy.
5) Mode-based design is an incremental design technique, where a design first starts with a single mode and gradually introduces other modes until the design criteria are met. Hence, mode-based design delivers the simplest design. On the other hand, configuration-based design determines the number of clutches beforehand and tries to find the best designs with a fixed number of clutches.
6) Since mode-based design is an incremental design technique, it is a straight-forward way to augment the superior designs with other modes to satisfy additional criteria. How to expand a design in the configuration-based design, however, is not clear.

III. PROPOSED DESIGN PROCESS

In any design task, the most critical step is to establish the design framework, because its guidelines have a major effect on the design space coverage, flexibility, and computational complexity. Fig. 3 shows the proposed process for designing a superior HEV transmission in terms of performance and fuel economy. The steps in this process and strategic thinking behind them can be summarized as follows. First, the design space is populated with the modes that can be generated with two PGs, one engine, one vehicle output shaft, two electric machines, and at most three brakes. Mode-based design makes the size of the design space manageable. Second, speed and torque equations for each mode are derived in a format such that computationally efficient vector operations can be performed for component-sizing studies. Then, the infeasible modes that are determined according to the speed and torque equations are removed from the design space. Third, feasible modes are classified according to the structure of their torque and speed equations so that proper analysis techniques specific to each powertrain type can be applied. Fourth, the modes are categorized into forward-speed and backward-speed groups, where forward-speed capable means that positive engine torque propels the vehicle in the forward direction. Fifth, the modes that cannot pass any of the predefined performance tests with any PG gear ratio combination are eliminated. Applying the challenging performance tests early in the process makes the design space

much smaller for further processing. Sixth, the individual modes or mode pairs that can meet all performance criteria collectively for the same PG ratios are identified to establish the core of the competent designs. Seventh, the clutch numbers and their locations are determined to achieve the transition between two modes in each competent mode pair. The other modes that can be generated for each combination of clutch states are also identified and analyzed. If any of these modes does not provide backward-speed capability, any mode in the backward-speed capable group that can be transitioned without exceeding the clutch number constraint is incorporated into the design. At the end of this stage, all competent designs have been identified. In the last step, the fuel economy improvement potential of these competent designs for each valid PG ratio is evaluated. Since these designs had to pass many demanding performance design criteria beforehand, computationally complex fuel economy analysis can be applied to a limited number of designs. Finally, the competent designs with superior fuel economy become the end product of the proposed process.

IV. DERIVATION OF STEADY-STATE AND DYNAMIC EQUATIONS

A goal of the design process should be to identify as many mode characteristics as possible by analyzing speed and torque equations at steady-state instead of dynamic equations because speed and torque equations at steady-state are in a simpler form, making them suitable for the vector operations and the derivation of important results in the design process. In this study, steady-state speed and torque equations are used in the feasibility, powertrain type, maximum vehicle torque, long-hauling capability, and forward/backward speed capability analyses since these calculations are performed only at a single time instant. However, dynamic equations are required in the *x*-*y* mph time and fuel economy simulations because each of them is performed multiple times sequentially on a time horizon. With the proposed method in subsection IV-B, dynamic equations can be easily obtained from speed and torque equations at steady-state.

A. DERIVATION OF SPEED AND TORQUE EQUATIONS AT STEADY-STATE

The high number of modes in the design space requires the automatic derivation of speed and torque equations. This task is accomplished by adapting the method in [20] to HEV powertrains. The proposed procedure generates all speed and torque equations and constraints due to the brakes and connections between PGs in a matrix form, thus facilitating the automation of the process. The procedure is explained using an example mode in Fig. 4. This example mode consists of all connection types (fixed connections between PGs, brake connection, and coaxial actuator connection to a PG node). Hence, the steps explained for this example are applicable to the modeling of other modes. The only differences in other modes are the number of rows in the matrix and the locations of 1's and −1's on each row. In the example mode, electric

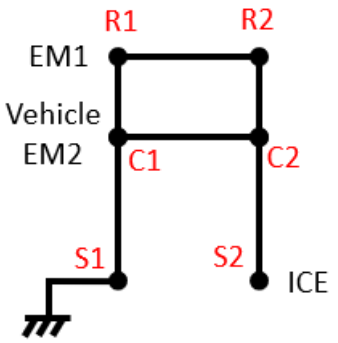

FIGURE 4. Example mode used in the derivation of speed and torque equations at steady-state.

machines 1&2 are connected to the ring and carrier nodes of the first PG, respectively. The vehicle output shaft, hereinafter referred to as "Vehicle," is on the same node as electric machine 2. The brake on the sun gear of the first PG keeps it at zero speed. The engine, hereinafter called "ICE," is connected to the sun gear of the second PG, with ring and carrier gears of both PGs connected to each other.

1) DERIVATION OF SPEED EQUATIONS

The first step in deriving the speed equations is to create the speed vector in (1) that multiplies the speed matrix. The speed vector consists of all six nodes of two PGs and the speed of the component that shares a node with another component (viz. electric machine 2). The first two rows of the speed matrix in (1) represent the speed equations of two PGs. The third and fourth rows are connection constraints, which make the PG1 ring and carrier speed equal to the PG2 ring and carrier speed. The fifth row shows the speed constraint imposed by the brake on the PG1 sun gear. The goal of the last row is to equate the speed of the components that are connected to the same node.

$$\underbrace{\begin{bmatrix} \theta_1 & -(1+\theta_1) & 1 & 0 & 0 & 0 & 0 \\ 0 & 0 & 0 & \theta_2 & -(1+\theta_2) & 1 & 0 \\ 1 & 0 & 0 & -1 & 0 & 0 & 0 \\ 0 & 1 & 0 & 0 & -1 & 0 & 0 \\ 0 & 0 & 1 & 0 & 0 & 0 & 0 \\ 0 & 1 & 0 & 0 & 0 & 0 & -1 \end{bmatrix}}_{\textit{Speed Matrix}} \underbrace{\begin{bmatrix} \omega_{EM1} \\ \omega_{Vehicle} \\ \omega_{S1} \\ \omega_{R2} \\ \omega_{C2} \\ \omega_{ICE} \\ \omega_{EM2} \end{bmatrix}}_{\textit{Speed Vector}} = 0 \tag{1}$$

2) DERIVATION OF TORQUE EQUATIONS

The torque vector consists of the elements that actively or reactively behave as a source of torque (i.e., electric machines, engine, vehicle output shaft, brakes, connections, and reaction forces in the PGs). In contrast to building the speed matrix, the torque matrix is established column by column.

Each row of the matrix corresponds to one of the nodes. Thus, the row size of the matrix is always 6 for a 2-PG design. For each row, the torque sources that act on the corresponding node of that row are set to 1 or -1, depending on the direction. The remaining elements in that row are set

to 0. According to these rules, the torque equations of the example mode become as in (2), where F_1 and F_2 are the tangential forces between gears in each PG, T_{C1} and T_{C2} are connecting torques between PGs, and T_B is the reaction torque exerted by the brake.

$$\begin{array}{c} \textit{Torque Matrix} \\ \begin{array}{c} R_1 \\ C_1 \\ S_1 \\ R_2 \\ C_2 \\ S_2 \end{array} \left[\begin{array}{ccc|ccccc} \theta_1 & 0 & 0 & 0 & 1 & 0 & 0 \\ -(1+\theta_1) & 0 & 0 & 1 & 0 & 1 & 0 \\ 1 & 0 & 0 & 0 & 0 & 0 & 1 \\ 0 & \theta_2 & 0 & 0 & 0 & -1 & 0 \\ 0 & -(1+\theta_2) & 0 & 0 & 0 & 0 & -1 \\ 0 & 1 & 1 & 0 & 0 & 0 & 0 \end{array}\right] \end{array}$$

$$\begin{array}{c} \textit{Torque Vector} \\ \cdot \begin{bmatrix} F_1 \\ F_2 \\ T_{ICE} \\ T_{Vehicle} \\ T_{EM1} \\ T_{EM2} \\ T_{C1} \\ T_{C2} \\ T_B \end{bmatrix} = 0 \end{array} \tag{2}$$

B. DERIVATION OF DYNAMIC EQUATIONS

The dynamic equations of a mode in this paper are used in the 0-60mph time analysis and fuel economy simulations. They are derived by combining the speed and torque equations at steady-state with the inertia matrix as follows.

First, the derivative of the speed vector in the speed equations is augmented by the torque vector in the torque equations to obtain the variable vector Ω of the dynamic equations. The variable vector Ω of the example in Fig. 4 becomes (3). The inertia matrix J is created first as a zero matrix, with a size of $6 \times N$, where N is the dimension of the speed vector and each row corresponds to one of the PG nodes. Each of the first six diagonal elements of the inertia matrix is populated with the sum of the inertia terms of the components connected to the corresponding node. Finally, the dynamic equation matrix is created by placing the inertia matrix, speed matrix, and torque matrix into its upper left, lower left, and upper right corners, respectively, as in (4). The torque matrix is multiplied by -1 before this placement, as inertia and torque matrices are on the same side of the dynamic equations.

$$\Omega = [\dot{\omega}_{EM1}\ \dot{\omega}_{Vehicle}\ \dot{\omega}_{S1}\ \dot{\omega}_{R2}\ \dot{\omega}_{C2}\ \dot{\omega}_{ICE}\ \dot{\omega}_{EM2}\ F_1\ F_2\ T_{ICE}\ T_{Vehicle}\ T_{EM1}\ T_{EM2}\ T_{C1}\ T_{C2}\ T_B]^T \tag{3}$$

$$\left[\begin{array}{c|c} J & -\textit{Torque Matrix} \\ \hline \textit{Speed Matrix} & 0 \end{array}\right] \Omega = 0 \tag{4}$$

V. FEASIBILITY ANALYSIS AND POWERTRAIN TYPE DETERMINATION

A. FEASIBILITY CHECK USING TORQUE EQUATIONS

The columns of the torque equation matrix are reordered so that the first and second columns of the matrix belong to $T_{Vehicle}$ and T_{ICE}. Gaussian elimination is then applied and the resultant first row is analyzed. If all elements after the first 1 are all zero, it follows that $T_{Vehicle}$ is always 0 and thus no torque is transmitted to the vehicle output shaft. As this is an infeasible condition for a powertrain design, no further investigation is needed.

B. FEASIBILITY CHECK USING SPEED EQUATIONS

The columns of the speed equation matrix are reordered so that the first column of the matrix belongs to $\omega_{Vehicle}$ and the last three columns belong to ω_{EM1}, ω_{EM2}, and ω_{ICE}, respectively. Gaussian elimination is then applied and the resultant first row is analyzed. If the remaining elements after the first 1 are all zero, that means that $\omega_{Vehicle}$ is always 0 and the mode is infeasible.

C. POWERTRAIN TYPE DETERMINATION

The remaining modes after eliminating the infeasible modes from the design space, called feasible modes, need to be categorized according to their powertrain type to apply the suitable analysis techniques and to meet the design criteria. Powertrain types are determined according to the source of the propulsion (full-electric, hybrid-electric, conventional) and the dependence of engine and electric machine speeds on vehicle speed (fixed-gear, parallel, series, power-split). In the literature, they are described in terms of the characteristics of the existing designs or ad-hoc results or fixed number of PGs [16], [21]–[25]. In this paper, the characteristics of all possible powertrain types that can be constructed with any number of PGs will be shown mathematically. In this way, any mode that might belong to an unknown powertrain type will not be ignored.

Proposition 1: The sum of the number of free variables (degrees of freedom) in steady-state torque and speed equations is equal to the number of power generating/consuming components in a powertrain design.

Proof: Assume there are m power generating/consuming components and the speed values of k components determine the rest of the speed variables via the matrix $A_{m-k\times k} = [a_1 \dots a_k]$ where a_i's are the columns of the A matrix. Using the energy conservation law,

$$[T_1\ \dots\ T_k\ T_{k+1}\ \dots\ T_m] \cdot \begin{bmatrix} \omega_1 \\ \vdots \\ \omega_k \\ \omega_{k+1} \\ \vdots \\ \omega_m \end{bmatrix} = 0 \tag{5}$$

$$[T_1\ \dots\ T_k\ T_{k+1}\ \dots\ T_m] \cdot \begin{bmatrix} I_{k\times k} \\ A_{m-k\times k} \end{bmatrix} \cdot \begin{bmatrix} \omega_1 \\ \vdots \\ \omega_k \end{bmatrix} = 0 \tag{6}$$

$$[T_1 + [T_{k+1} \dots T_m] \cdot a_1 \dots T_k + [T_{k+1} \dots T_m] \cdot a_k] \cdot \begin{bmatrix} \omega_1 \\ \vdots \\ \omega_k \end{bmatrix} = 0 \tag{7}$$

TABLE 1. Feasibility and powertrain type determination analyses results.

	1-Connection	2-Connection
Total Number of Modes	36,000	13,824
Feasible Modes	24,228	10,152
Powertrain Type		
Fixed Gear	2,988	432
EV	5,364	216
Parallel	8,712	6,480
Series	2,232	432
Input-Split	1,368	864
Output-Split	1,368	864
Compound-Split	0	432
Special Power-Split	2,196	432

Since $\omega_1, \ldots, \omega_k$ are independent variables, $T_i + \left[T_{k+1} \ldots T_m\right] \cdot a_i, i = 1, ..., k$ terms should be 0. As a result, $m - k$ variables $T_{k+1}, ..., T_m$ are independent torque variables. ■

This result is applied to the design process as follows. The columns of the speed and torque equation matrices are reordered so that their first columns belong to the vehicle output shaft and their last three columns belong to the electric machines 1 and 2 (EM1, EM2), and the engine. After the Gaussian elimination method is applied to these matrices, the free variables are obtained. For the feasible modes, three cases are possible where k and n are the number of free speed and torque variables among Vehicle, Engine, EM1, and EM2, respectively:

1) $k = 1, n = 3$
2) $k = 3, n = 1$
3) $k = 2, n = 2$

Figs. 5-9 show the algorithms that determine all possible powertrain types in the design space through a systematic approach. The derivation of these algorithms relies heavily on two facts. The first one is the energy conservation law the way it is used in the proof of Proposition 1. The second one is the property of reduced row echelon form, where each leading entry (left most nonzero entry) of a row is in a column to the right of the leading entry of the row above it. For example, if ω_{EM1} and ω_{ICE} are the free variables in the reduced row echelon form of a speed matrix, ω_{EM2} should be either 0 or $a \cdot \omega_{ICE}$ since these variables are ordered in the last three columns of the speed matrix as ω_{EM1}, ω_{EM2}, and ω_{ICE}, respectively. After the implementation of feasibility and powertrain type determination algorithms, the powertrain types listed in Table 1 are identified.

The important results these algorithms provide are as follows.

1) The characteristics equations of each powertrain type are converted to a common format, to which the analysis techniques in the design process are applied seamlessly.
2) All powertrain types achievable with the given set of components can be identified mathematically, regardless of the number of PGs. For example, a new special power-split powertrain type, where T_{ICE} is determined only by $T_{Vehicle}$, while ω_{ICE} is a function of $\omega_{EM1/2}$ and $\omega_{Vehicle}$, is uncovered thanks to this method. Two examples of this power-split powertrain type are shown in Fig. 10.

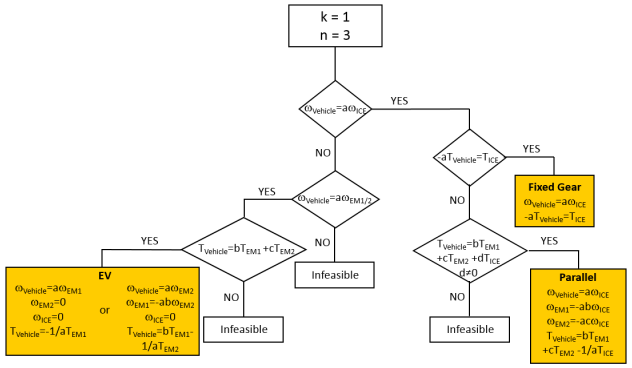

FIGURE 5. Flow Chart to determine Powertrain Type for $k = 1$, $n = 3$.

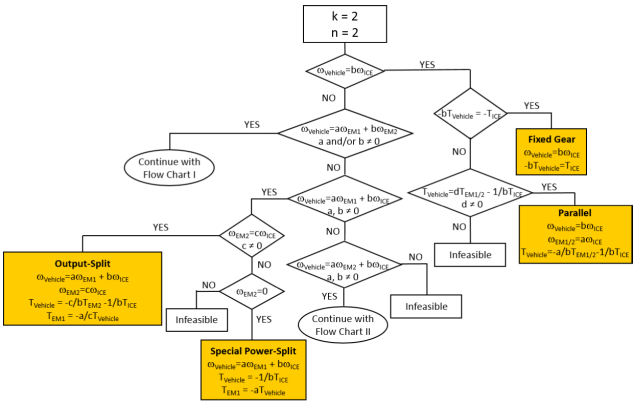

FIGURE 6. Main Flow Chart to determine Powertrain Type for $k = 2$, $n = 2$.

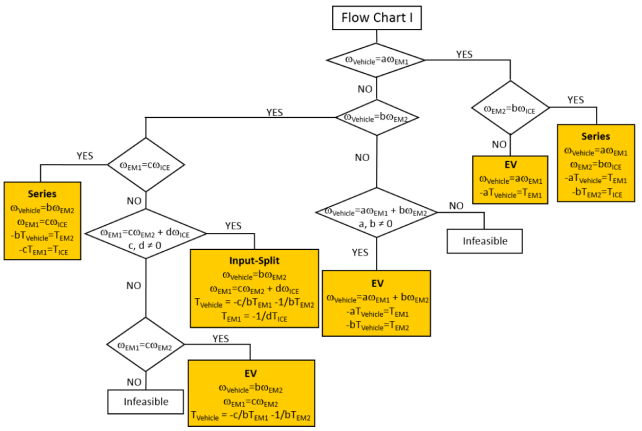

FIGURE 7. Flow Chart I to determine Powertrain Type for $k = 2$, $n = 2$.

VI. MODE EVALUATION WITH RESPECT TO PG RATIOS

Feasibility and powertrain type analyses can be performed for one set of PG ratios since the structure of the equations is sufficient for drawing conclusions. However, the successive

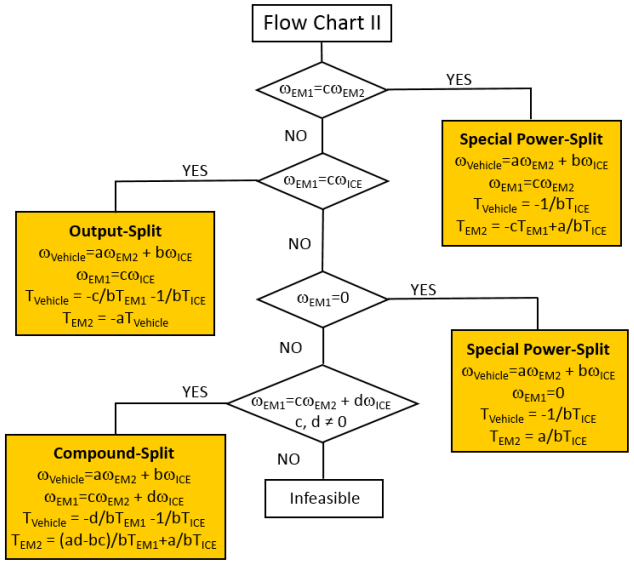

FIGURE 8. Flow Chart II to determine Powertrain Type for $k = 2$, $n = 2$.

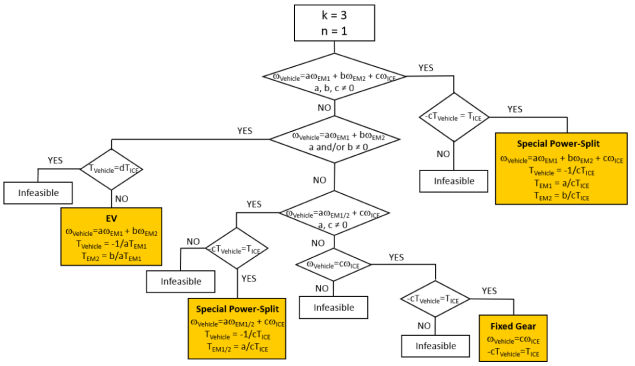

FIGURE 9. Flow Chart to determine Powertrain Type for $k = 3$, $n = 1$.

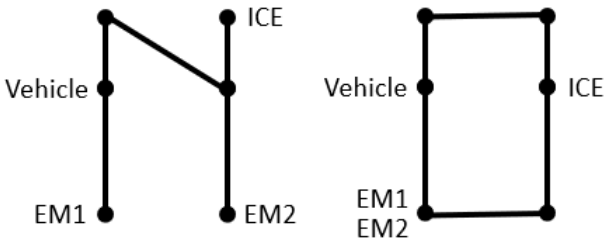

FIGURE 10. Two Examples of Special Power-split Powertrain Type.

analyses in the design process require the evaluation of the feasible modes for each PG gear ratio combination since the value of the PG gear ratio affects the analysis outcomes. Due to the computational burden of introducing PG ratios into the design process, either constant PG ratios are assumed or a smaller design space is used in the literature.

In this paper, the speed and torque equations derived in the powertrain type determination algorithms are used in the performance analyses because they are functions of PG gear ratios and suitable for fast vector operations. These PG gear ratio dependent equations are obtained in three steps. First, speed and torque matrices explained in Section IV are generated using Matlab Symbolic Toolbox by defining the PG gear ratios as symbolic variables. Second, the Gaussian elimination method is applied to these matrices as described in Subsection V-C to calculate speed and torque equations in symbolic form, which are later converted into a string. Third, PG gear ratios are discretized with 0.1 increments in the physically feasible range of [1.8, 3.8] [26], and all PG gear ratio combinations in the vector form are applied as inputs to the symbolic equations in the string format using Matlab's "eval" command. As a result, this methodology allows us to perform all mode performance analyses for all PG gear ratio combinations with minimal computational impact.

VII. FORWARD/BACKWARD SPEED CAPABILITY CHECK

After categorizing the feasible modes according to the powertrain types, whether positive engine torque contributes to the forward or backward motion of a vehicle is determined for each mode, as backward motion can be achieved at a low battery state of charge if and only if the engine is on.

For this purpose, the torque equation $T_{Vehicle} = f_1(\theta_1, \theta_2) \cdot T_{EM1} + f_2(\theta_1, \theta_2) \cdot T_{EM2} + f_3(\theta_1, \theta_2) \cdot T_{ICE}$, where f_1, f_2, and f_3 coefficients are functions of PG gear ratios is used. If $f_3 < 0$ for the PG gear ratio combination, positive T_{ICE} will propel the vehicle in the forward direction because negative $T_{Vehicle}$ representing the load to the system corresponds to vehicle acceleration. Similarly, if $f_3 > 0$, positive T_{ICE} will support backward motion. As a result, each mode is assigned to either of forward-speed and backward-speed capable groups or both, depending on the sign change of f_3 for different PG ratios.

VIII. PERFORMANCE EVALUATIONS

In the HEV design literature, performance criteria other than 0-60mph time have been overlooked due to either lack of experience in the automotive industry or algorithm simplification. Therefore, the results of the design processes may not have shown any practical value. Moreover, 0-60mph time is calculated with assumptions that degrade the accuracy of the results. In this paper, we introduce not only analyses related to the performance criteria necessary for designing a marketable vehicle but also an accurate 0-60mph time calculation method.

The performance criteria have been determined based on the SAE J2807 Standard and general design requirements in the automotive industry for a vehicle at its Gross Combination Weight Rating (GCWR). They are categorized into three groups (see Table 2 for details). In the evaluation of long-hauling capability, maximum output torque of the HEV powertrain is calculated under the assumption of charge sustaining operation, whereas in the gradeability and x-y mph time calculations, the only constraint is the limits of the components in the design.

TABLE 2. Performance criteria.

Gradeability	Long-Hauling Capability	x-y mph Time
15% at 6 mph	8% at 25 mph	0-60 mph Time $\leq$ 20s
12% at 12 mph	6% at 40 mph	0-30 mph Time $\leq$ 10s
0% at 113 mph	4% at 50 mph	40-60 mph Time $\leq$ 10s
	2% at 75 mph	

A. LONG-HAULING CAPABILITY ANALYSIS

In the long-hauling performance analysis, the maximum vehicle output torque of each mode without depleting the battery is calculated for each PG ratio combination. This calculation is simple for powertrain types with one degree of freedom in speed equations such as fixed gear, parallel, and series. For these types, engine or electric machine speed is easily calculated from the vehicle speed, and using speed vs. maximum torque curves of the related component, maximum vehicle output torque is obtained. Difficulty arises for powertrain types with more than one degree of freedom because engine speed can be controlled independent of vehicle speed. In this section, the method derived for modes with two degrees of freedom (input-split, output-split, and compound-split) is given in detail. Since the approach is the same for the modes with three degrees of freedom, their derivations are skipped.

Steady-state speed and torque equations of power-split types with two degrees of freedom can be written as in (8a)-(8d), where f_1, f_2, g_1, g_2 are the column elements in the first two rows of the speed matrix that correspond to ω_{ICE} and $\omega_{Vehicle}$ and f_3, f_4, g_3, g_4 are the elements in the torque matrix that correspond to T_{ICE} and $T_{Vehicle}$. In addition to regenerative braking and torque assist, the main task of electric machines in a power-split hybrid powertrain is to provide electronically controlled continuously variable transmission (eCVT) operation, where the engine can run with the control of electric machines at the highest system efficiency point independent of vehicle speed. Since the vehicle is supposed to operate at cruising vehicle speed levels in the eCVT mode for long durations and the battery has limited charge, it is assumed that net energy transfer from/to battery is 0 in the eCVT operation and the energy generated by one of the electric machines is consumed by the other electric machine. Furthermore, lossless electric machines, that is, $P_{EM1} = -P_{EM2}$, are assumed because in the long-hauling analysis the maximum output power of the vehicle is calculated, where electric machines operate at power levels close to their highly efficient maximum values. Under this assumption, (8a)-(8d), and energy conservation law, the electric machine power to engine power ratio is calculated as in (9), where $x = \frac{\omega_{Vehicle}}{\omega_{ICE}}$. Since $P_{ICE} = -P_{Vehicle}$ in the batteryless eCVT operation and (9) is suitable for vector operations, the electric machine power requirement of all modes with their PG gear ratio combinations can be calculated very quickly for the given road loads in Table 2. If P_{EM1} is less than the maximum electric machine power for a given long-hauling requirement, then the mode with its corresponding PG gear ratios is recorded as a capable mode.

$$\omega_{EM1} = f_1(\theta_1, \theta_2)\omega_{ICE} + g_1(\theta_1, \theta_2)\omega_{Vehicle} \quad (8a)$$

$$\omega_{EM2} = f_2(\theta_1, \theta_2)\omega_{ICE} + g_2(\theta_1, \theta_2)\omega_{Vehicle} \quad (8b)$$

$$T_{EM1} = f_3(\theta_1, \theta_2)T_{ICE} + g_3(\theta_1, \theta_2)T_{Vehicle} \quad (8c)$$

$$T_{EM2} = f_4(\theta_1, \theta_2)T_{ICE} + g_4(\theta_1, \theta_2)T_{Vehicle} \quad (8d)$$

$$\frac{P_{EM1}}{P_{ICE}} = \frac{f_3 g_1 x^2 + (f_1 f_3 - g_1 g_3)x + -f_1 g_3}{x} \quad (9)$$

B. MAXIMUM OUTPUT TORQUE ANALYSIS

In the gradeability and x-y mph time evaluations, the maximum output torque that a mode can deliver without the battery state of charge constraint in the long-hauling capability analysis needs to be calculated. Similar to the long-hauling analysis, the speed and torque of both the engine and the electric machines must be optimized for powertrain types with more than one degree of freedom. Due to the computational difficulty of this optimization problem, in the literature it has been performed by either unjustified assumptions for problem simplification [13] or brute force [14], which is not computationally feasible when the PG gear ratio is a design variable.

In this study, the speed and torque relationships of the components are formulated such that a linear programming technique can be applied. The variables in the linear program are ω_{EM1}, ω_{EM2}, ω_{ICE}, $\omega_{Vehicle}$, T_{EM1}, T_{EM2}, T_{ICE}, and $T_{Vehicle}$. Although upper and lower speed limits of the electric machines and engine are constant, as in (10a)-(10d), their torque limits are a function of their speed. Thus, a special formulation suitable to linear programming is needed to ascertain the torque limits.

$$-\omega_{EM1max} \leq \omega_{EM1} \leq \omega_{EM1max} \quad (10a)$$

$$-\omega_{EM2max} \leq \omega_{EM2} \leq \omega_{EM2max} \quad (10b)$$

$$\omega_{ICEmin} \leq \omega_{ICE} \leq \omega_{ICEmax} \quad (10c)$$

$$0 \leq \omega_{Vehicle} \leq \omega_{Vehiclemax} \quad (10d)$$

In the formulation of engine torque limits, the maximum torque curve of an engine can be approximated as a combination of linear segments with decreasing slopes. The maximum torque curve of the engine used in this paper is shown in Fig. 11 as the blue line. The original curve is approximated by three line segments ($a_i\omega_{ICE} + b_i$, $i = 1, 2, 3$) concatenated to each other, shown as the red line in the same figure. The resulting upper and lower limits of the engine torque can be represented as:

$$0 \leq T_{ICE}(\omega_{ICE}) \leq \min_i(a_i\omega_{ICE} + b_i) \quad i = 1, 2, 3 \quad (11)$$

In formulating the electric machine torque limits, the approach taken is the same as that with the engine torque limits. In contrast to engines, however, electric machines are capable of producing large negative torque. As the minimum torque curve of an electric machine is generally a reflection of its maximum torque curve around the speed axis (x-axis), the formulation of the maximum torque curve of an electric

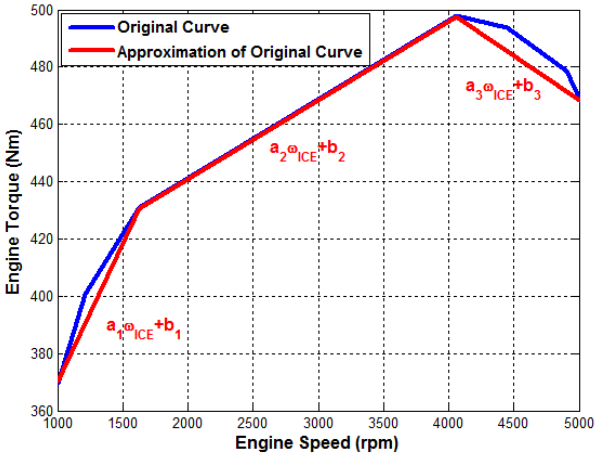

FIGURE 11. Maximum engine torque curve.

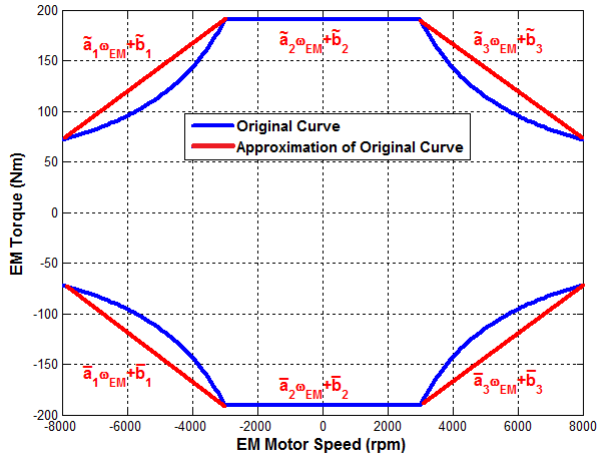

FIGURE 12. Max. and Min. electric machine torque curves.

machine can be applied to the representation of its minimum torque curve. The maximum and minimum torque curves of the electric machines used in this paper are shown as the blue lines in Fig. 12. Although maximum (minimum) torque curve is not a concave (convex) function of the machine speed, it can be approximated as a concave (convex) function by concatenating three line segments ($\tilde{a}_i\omega_{EM}+\tilde{b}_i, i=1,2,3$ for the maximum torque curve and $\bar{a}_i\omega_{EM}+\bar{b}_i, i=1,2,3$ for the minimum torque curve), as shown by the red lines in Fig. 12. This approximation is legitimate, as electric machines can exceed their limits temporarily as long as overheating is prevented. With this approximation, the electric machine torque limits are represented as:

$$\max_i(\bar{a}_i\omega_{EMj}+\bar{b}_i) \le T_{EMj}(\omega_{EMj}) \le \min_i(\tilde{a}_i\omega_{EMj}+\tilde{b}_i) \quad i=1,2,3 \;\; j=1,2 \tag{12}$$

The interdependencies between the speed and torque values of the engine, vehicle output shaft, and electric machines are obtained by applying the Gaussian elimination method to the speed and torque matrices. For the powertrain types with

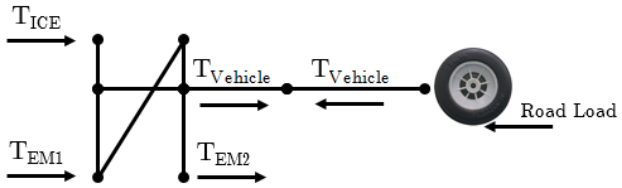

FIGURE 13. Maximum acceleration formulation.

two degrees of freedom (input-split, output-split, compound-split), speed and torque equations can be represented as in (8a)-(8d) of Subsection VIII-A.

In the linear program, $\omega_{Vehicle}$ is set to the vehicle speed at which the vehicle begins its acceleration. In the formulation, the $T_{Vehicle}$ term is the reaction torque of the PG node to which the output shaft is connected, as shown in Fig. 13. In this figure, arrows facing right represent positive torque. Maximum acceleration is achieved if $T_{Vehicle}$ is minimized. Thus, the objective of the linear program is to minimize $T_{Vehicle}$ within the speed and torque constraints of the components described through (8a)-(8d), (10a)-(10d), and (11)-(12) for the input-split-, output-split-, and compound-split powertrain types. For the special power-split powertrain types, torque and speed equations are those shown in Figs. 6, 8, and 9. In the formulation, it is assumed that the speed of the components has already been settled to the speed solutions of the linear program at the start of acceleration, and that the torque solutions of the linear program are applied to the actuators at these speed points.

C. x-y mph TIME CALCULATION

The linear program formulation from the previous subsection is used for the x-y mph time calculation. The algorithm must be modified, however, due to the dynamic nature of the x-y mph acceleration. It is assumed that the vehicle begins its acceleration at a vehicle speed of x, while the speeds of the engine and electric machines are at the values calculated by the linear program for maximum acceleration. Furthermore, the inertias of the ring, carrier and sun gears of the PGs and two electric machines are assumed to be 0 since they are much smaller than the vehicle inertia and engine inertia.

In the algorithm, the feasible engine torque region is constrained between $T_{ICEmax}-\Delta T_{ICEmax}$ and $T_{ICEmin}+\Delta T_{ICEmax}=\Delta T_{ICEmax}$ assuming $T_{ICEmin}=0$. ΔT_{ICEmax} is the reserve torque needed to bring the engine speed to the desired level at the beginning of the next simulation time step. ΔT_{ICEmax} can be calculated by $J_{ICE}\Delta\omega_{ICEmax}$, where J_{ICE} is engine inertia and $\Delta\omega_{ICEmax}$ is the maximum difference between optimum engine speed setpoints at two consecutive time steps.

The algorithm works in the following order:

1) Start at $k\Delta t=0$ and $\omega_{Vehicle\_k}=x$, where Δt is the duration of each time step.
2) Solve the linear program that minimizes $T_{Vehicle\_k}$ within the $T_{ICEmax}-\Delta T_{ICEmax}$ curve. The solution of

the linear program is ω_{ICE_k}, T_{EM1_k}, T_{EM2_k}, T_{ICE_k} and $T_{Vehicle\_k}$.

3) Using the road load model and $T_{Vehicle\_k}$, predict the vehicle speed $\omega_{Vehicle\_k+1}$ at the start of the next time step $(k+1)$.
4) Solve the linear program for this predicted vehicle speed $\omega_{Vehicle\_k+1}$. The solution gives the desired ω_{ICE_k+1} at the end of the current time step k.
5) Calculate engine torque command T_{ICEcmd_k} applied at $k\Delta t$ that brings ω_{ICE_k} to ω_{ICE_k+1} using $T_{ICEcmd\_k} - T_{ICE\_k} = J_{ICE}(\omega_{ICE\_k+1} - \omega_{ICE\_k})$. Verify that T_{ICEcmd_k} is inside the T_{ICEmax} curve. If not, restart the algorithm after increasing ΔT_{ICEmax}.
6) Apply the torque command to the engine and increment k by 1 and repeat steps 2-5.
7) Once the vehicle speed reaches y mph, stop the process and calculate total acceleration time.

This algorithm is executed for all modes at each simulation time step, and the time at every 10mph interval is recorded.

D. POWERTRAIN TYPE SPECIFIC LP SOLVER

In the 0-60mph time calculation, assuming the simulation period is 0.1s and the fully loaded vehicle reaches 60mph in 20s, LP solver in Matlab will be called 88, 200 times for a single mode, if we consider 441 PG gear ratio combinations. For a design space with hundreds of modes, 0-60mph time calculation takes too much time and therefore, is not feasible. In this section, an efficient LP solver designed for the powertrain types is presented.

A computationally efficient LP solver should have two characteristics: the solution should be able to be found quickly and it should be suitable for vector operations to accommodate PG gear variations. In the proposed method, the optimum solution is found by leveraging the fact that the LP solution is always associated with a corner point (where two lines intersect) of the solution space [27]. Moreover, the speed and torque equations and solution algorithm are constructed such that all mathematical operations can be performed in vector form without the use of any ''for'' loop.

The fundamental steps of the LP solver are described in seven steps with the accompanying example of an input-split mode, whose speed and torque equations are given in (13)-(14).

1) Represent maximum torque equations of all components in terms of a single variable using speed equations $T_{x,max} = \min_i(a_{x,i}\omega_{ICE} + b_{x,i}) \quad i = 1, 2, 3$ and $x \in \{ICE, EM1, EM2\}$. This is achievable since input-split, output-split, compound-split and some special power-split powertrain types have two-degrees of freedom in speed equations and the LP solver is executed for a specific vehicle speed.
2) Perform the same operation for the minimum torque curves of the components. For the example mode, maximum and minimum torque curves of the components are plotted in Fig. 14 for $\omega_{Vehicle} = 0$, assuming the vehicle is starting its acceleration.
3) Determine all speed points, where the maximum/minimum torque curve of each component changes its slope. These points are the optimum solution candidates. The black-yellow circle markers in Fig. 14 correspond to these points of the example mode.
4) Minimize $T_{Vehicle}$ by setting the independent torque variables to their maximum or minimum values. In the example mode, independent torque variables are T_{EM1} and T_{EM2}. Assuming $b(\theta_1, \theta_2)$ and $c(\theta_1, \theta_2)$ coefficients are positive, T_{EM1max} and T_{EM2max} would minimize $T_{Vehicle}$.
5) Using the values of the independent torque variables set in the previous step, calculate the torque values, which the remaining components must reach. The black curve in Fig. 14 shows the engine torque determined by T_{EM1max} as $T_{ICEreq} = -d(\theta_1, \theta_2)T_{EM1max}$. However, T_{ICEreq} is larger than T_{ICEmax} in the first half of the curve. In this case, the limiting variable is T_{ICEmax} and T_{EM1} should be $-\frac{1}{d(\theta_1,\theta_2)}T_{ICEmax}$ instead of T_{EM1max}. The red-blue circle markers in Fig. 14 correspond to the solution candidates at corner points determined according to this procedure.
6) Determine the speed point, at which the limit of the dependent torque variable is equal to the requested torque set by the independent torque variables that minimize $T_{Vehicle}$. This speed point is calculated geometrically by first identifying two intersecting line segments that belong to the component maximum/minimum torque curve and the requested torque curve and then solving the linear equations for the intersection point. In the Fig. 14, the blue-light blue circle marker corresponds to this corner point, where $T_{ICEmax} = T_{ICEreq} = -d(\theta_1, \theta_2)T_{EM1max}$.

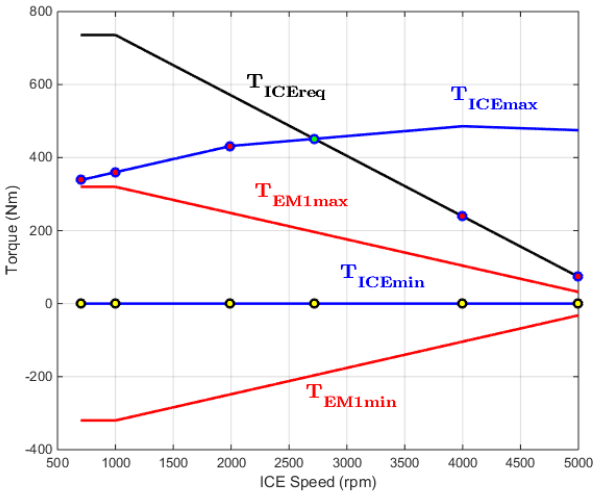

FIGURE 14. Maximum/Minimum torque curves of ICE, EM1, and EM2 as a function of ω_{ICE}.

7) Choose the minimum of $T_{Vehicle}$s obtained at each of these corner points as the optimum solution.

All of the steps above can be performed in vector form, that is, each step can be evaluated for all PG ratio combinations in one operation. Therefore, the introduced LP solver is much faster than Matlab's LP solver and enables the accelerated evaluation of gradeability and x-y mph time of a large design space.

The algorithm described here must be slightly modified for some special power-split modes with three degrees of freedom in speed variables. In this case, the maximum/minimum torque curves of the components cannot be represented by a single speed variable, although one variable $\omega_{Vehicle}$ is constant. This problem can be reduced to the case of two degrees of freedom by executing the LP solver procedure above for each maximum T_{ICEmax} linear segment. For each linear segment, there would be one more corner point, where the maximum/minimum curves of three components intersect, that is, $T_{ICEmax/min} = \frac{c}{a}T_{EM1max/min}$ and $T_{ICEmax/min} = \frac{c}{b}T_{EM2max/min}$.

$$\begin{aligned} \omega_{Vehicle} &= b(\theta_1,\theta_2)\omega_{EM2} \\ \omega_{EM1} &= c(\theta_1,\theta_2)\omega_{EM2} + d(\theta_1,\theta_2)\omega_{ICE} \end{aligned} \tag{13}$$

$$\begin{aligned} T_{Vehicle} &= -\frac{c(\theta_1,\theta_2)}{b(\theta_1,\theta_2)}T_{EM1} - \frac{1}{b(\theta_1,\theta_2)}T_{EM2} \\ T_{ICE} &= -d(\theta_1,\theta_2)T_{EM1} \end{aligned} \tag{14}$$

IX. MODE GROUPING

The modes in the design space are grouped according to the PG node assignments of the vehicle, engine, EM1, and EM2 components in order to analyze mode transition feasibility through clutches. Since there are six PG nodes in a two-PG design, and vehicle and engine are not on the same node, $6 \times 5 \times 6 \times 6 = 1,080$ groups are possible. To assign each mode to its corresponding mode group(s), PG nodes are numbered zero to five, where zero to two numbers correspond to the ring, carrier, and sun gears of the first PG, respectively, and three to five numbers belong to the second PG. Furthermore, each component entry in the data structure created to hold mode information contains the PG node to which it is connected. The group number is created as a four-digit number in the heximal number system, as *Vehicle_Node|ICE_Node|EM1_Node|EM2_Node* as the maximum value of a four-digit heximal number (1295) is closest to 1, 080. It should be noted that a mode is assigned to more than one group if a component in the mode is connected to a PG node that has a mechanical connection with another PG node.

The advantage of such a numbering system in mode grouping is to be able to identify the symmetric topology of a mode and to skip the analysis of the mode with a higher group number because these two modes show exactly the same performance. Furthermore, if the group number generated by interchanging EM1 and EM2 node assignments is greater than the original group number, the analysis of the mode with the higher number is skipped, since EM numbering is just a convention and interchanging the EM numbers would not change the performance of a mode. This approach eliminates the need to analyze at least half of the mode groups that are functionally represented in other lower-number groups and accelerates the processing time.

TABLE 3. Gradeability matrix.

(θ_1,θ_2)	6 mph	12 mph	113 mph
$(1.8, 1.8)$	0/1	0/1	0/1
...	...	...	...
$(3.8, 3.8)$	0/1	0/1	0/1

TABLE 4. Long-hauling matrix.

(θ_1,θ_2)	25 mph	40 mph	50 mph	75 mph
$(1.8, 1.8)$	0/1	0/1	0/1	0/1
...	...	...	...	...
$(3.8, 3.8)$	0/1	0/1	0/1	0/1

TABLE 5. *x-y* mph time matrix.

(θ_1,θ_2)	$t_{0\text{-}60mph} \leq 20s$	$t_{0\text{-}30mph} \leq 10s$	$t_{40\text{-}60mph} \leq 10s$
$(1.8, 1.8)$	0/1	0/1	0/1
...	...	...	...
$(3.8, 3.8)$	0/1	0/1	0/1

X. IDENTIFICATION OF COMPETENT SINGLE-MODE AND TWO-MODE DESIGNS

After assigning each mode to its corresponding groups, each group is searched for a mode that meets all performance criteria. These modes are declared to be competent single-mode designs. If two modes in a group can meet all performance criteria together, the design that includes these two modes is called a competent two-mode design, although this design may also include other modes.

A. IDENTIFICATION OF COMPETENT SINGLE-MODE DESIGNS

During the performance evaluation of modes, gradeability matrix, long-hauling matrix, and x-y mph time matrix are generated for each mode, as shown in Tables 3-5, where each row and column correspond to a PG gear ratio combination and a specific performance criterion, respectively, and the value of 1 in a cell means the mode can meet the performance criterion. In order to identify the modes and their corresponding PG gear ratios that can meet all performance criteria, logical AND operation is applied along each row of the gradeability, long-hauling, and x-y mph time matrices. The result of this operation for each mode is gradeability-, long-hauling-, and x-y mph time vectors. Element-wise logical AND operation on these vectors produces the final competency vector, where the value of 1 in any of its rows means that the mode is competent for the PG ratios corresponding to that row.

After running these operations, two modes, all of which are input-split powertrain type are identified, which can meet all performance criteria.

TABLE 6. Combining the performance matrices of two modes.

Mode 1		Mode 2		
Gradeability Matrix 1	OR	Gradeability Matrix 2	=	Gradeability Matrix
Long-Hauling Matrix 1	OR	Long-Hauling Matrix 2	=	Long-Hauling Matrix
x-y mph Time Matrix 1	OR	x-y mph Time Matrix 2	=	x-y mph Time Matrix Matrix

TABLE 7. Evaluating the performance of combined two modes.

Column-wise AND of Gradeability Matrix	$\Rightarrow$	Gradeability Vector
Column-wise AND of Long-Hauling Matrix	$\Rightarrow$	Long-Hauling Vector
Column-wise AND of x-y mph Time Matrix	$\Rightarrow$	x-y mph Time Vector

TABLE 8. Generating the competency vector of combined two modes.

Gradeability Vector	AND	Long-Hauling Vector	AND	x-y mph Time Vector	=	Competency Vector	
						$\theta_1 = 1.8, \theta_2 = 1.8$	0/1
						...	...
						$\theta_1 = 3.8, \theta_2 = 3.8$	0/1

TABLE 9. Backward-speed performance criteria.

Criteria	Vehicle Speed	Vehicle Weight
15% Gradeability	0 mph	Gross Combination Weight Rating (GCWR)
15% Gradeability	-6 mph	Gross Combination Weight Rating (GCWR)
0% Gradeability	-10 mph	Gross Vehicle Weight Rating (GVWR)

B. IDENTIFICATION OF COMPETENT TWO-MODE DESIGNS

In a competent two-mode design, all performance requirements are met by either of the two modes in the design. The identification of these two modes starts with generating all two-mode combinations in each mode group. Then element-wise logical OR operation is performed on the gradeability-, long-hauling-, and x-y mph time matrices of two modes, as shown in Table 6. The resultant gradeability-, long-hauling-, and x-y mph time matrices show the capability of the mode pair. Afterwards, the same logical operations described in Subsection X-A are applied to these matrices, as shown in Tables 7 and 8. At the end of the process, a single competency vector is obtained, which shows at which PG gear ratio combination the mode pair is competent.

After the competency analysis, the number and location of clutches required to achieve mode transition between two modes is determined by comparing PG nodes to which components are connected in both modes. For example, if EM1 is connected to '0-4' (according to the numbering convention explained in Section IX) in one mode and '0' in the other mode, a clutch between the ring gear of the first PG and carrier gear of the second PG is needed for the mode transition. The clutch number limit for a mode transition is set to three to balance the tradeoff between design complexity and flexibility. The mode pairs from all mode groups that can meet the performance criteria and transition to each other with a maximum number of three clutches are collected with the PG gear ratio information to move to the next stages of the design process.

XI. IDENTIFICATION OF AUXILIARY MODES

In the process of identifying competent two-mode designs, the clutches required to make the mode transition possible are also determined. When more than one clutch is required for the transition, only two combinations of clutch states realize two competent modes. Therefore, other feasible modes can exist in the design for the remaining combinations of clutch states. These modes are called auxiliary modes since they are a by-product of the competent two-mode design process and do not contribute to meeting performance requirements. In this stage of the design process, the feasibility, speed and torque equations, and powertrain type of these auxiliary modes are explored using the analysis techniques in this paper so that their contribution to the performance and fuel economy can be taken into account.

XII. IDENTIFICATION OF BACKWARD-SPEED CAPABLE MODES

A powertrain design is incomplete without backward-speed capability. Another requirement often omitted in the literature is the need for a hybrid electric powertrain to be able to deliver propulsion with the engine in the backward direction in low battery SOC scenarios. Backward-speed capable modes that were identified in Section VII are assessed against the backward-speed performance criteria in Table 9. The modes that can meet the requirements are grouped according to the PG node assignments of the vehicle, engine, EM1, and EM2 components using the method explained in Section IX.

XIII. ADDITION OF BACKWARD-SPEED CAPABLE MODE TO THE COMPETENT DESIGNS

In the previous sections, the designs with one or two competent modes are explored. In this section, how these designs are mated with a competent backward-speed capable mode will be explained.

Single-mode designs do not have any additional mode to satisfy backward-speed performance criteria. Therefore,

a competent backward-speed capable mode is sought in the mode group to which the single mode design belongs. The acceptance criterion for a backward-speed capable mode in the single-mode design is that the number of clutches required to perform mode transition should not exceed the clutch number limit. At the end of this process, no any competent single-mode design that can be mated with a backward-speed capable mode is identified.

For designs with two competent modes, first the auxiliary modes of the design are evaluated in terms of backward-speed capability. If any of these modes meets the performance criteria, the design is complete and there is no need to explore any new mode. If any auxiliary mode of the design is not a backward-speed capable mode and the number of clutches in the design is less than the clutch number limit, then all backward-speed capable modes are analyzed in the mode groups of which the competent design is also a member. If the additional clutch(es) required to achieve the mode transition between forward- and backward speed capable modes does not cause the number of clutches to exceed the limit, the related backward-speed capable mode is made part of the design by adding the necessary clutches to the design. At the end of this process, 43 competent designs are identified.

XIV. FUEL ECONOMY ANALYSIS OF COMPETENT DESIGNS

Performance and fuel economy are two main pillars on which the design process is based. Thus far, the focus has been on the performance pillar, eliminating as many modes as possible from the design space and reducing the time for the fuel economy analysis. Since the designs that can meet all performance criteria are generated in the preceding section, in this section the fuel economy of each design for each competent PG ratio combination is evaluated.

The ideal method for analyzing fuel economy is Dynamic Programming (DP), as it guarantees global optimality over the problem horizon. DP suffers, however, from a heavy computation load and, hence, has been used only in studies with a small design space [11], [28], [29]. In the literature, several near-optimal fuel economy analysis methods have been introduced [30], [31]. In this study, one of these methods, called power-weighted efficiency analysis for rapid sizing (PEARS), will be used with some improvements.

The PEARS method first calculates the best power-weighted efficiency of each mode in the design for both EV and HEV operations at every vehicle speed and load point of the selected drive cycle. Then a DP algorithm over the time horizon of the drive cycle is executed to select a mode at every time point of the drive cycle with the goal of maximizing fuel economy. In this study, three improvements are made to this method. First, the algorithm is extended to include all special power-split powertrain types in the PEARS. Second, at the most efficient EV operating point calculation of each mode, all engine speed points between 0 and ω_{ICE} at 100rpm increments are taken into account instead of just three engine speed points as in the original method. Higher engine speed resolution allows the method to obtain an operating point close to the optimal one. Third, instead of the most efficient EV and HEV operating points of each mode, the most efficient points of each mode for EV, battery charging HEV, and battery discharging HEV operations are included in the mode selection DP execution. With this modification, the bandwidth of control inputs is increased for the mode selection DP, and the possibility of no solution for the competent single mode designs is avoided.

Using the modified PEARS, all competent designs are assessed in the Urban Dynamometer Driving Schedule (UDDS) and Highway Fuel Economy Test (HWFET) drive cycles for all feasible PG gear ratio combinations. Battery SOC is allowed to vary between 55% and 65% during simulations. Moreover, the battery SOC at the end of each cycle is kept the same as the SOC at the beginning of the cycle by penalizing the control actions that lead to an SOC mismatch. The weighted average of cycle results (55% UDDS and 45% HWFET) is calculated, and the PG gear ratio combination that gives the highest fuel economy is selected for comparison. Out of 43 designs, 22 are able to pass the 30mpg threshold. Ten of these designs are shown in Fig. 15. None of the 22 designs belongs to the one that met the performance criteria with a single mode, a finding that is expected, given that the limited number of modes in a design decreases the control bandwidth. The highest fuel economy achieved among the competent designs is 31.5mpg. The fuel economy of the same vehicle with a 6-speed automatic transmission instead of a hybrid electric powertrain is also simulated for a benchmark. The results show a fuel economy of 22.6mpg. Consequently, the maximum fuel economy improvement owed to a hybrid electric powertrain is 39%. A performance and fuel economy comparison of the designs in Fig. 15 and the conventional powertrain are shown in Figs. 16-17 and Table 11.

The following observations are made from the analysis of 43 competent designs, and their performance and fuel economy benefits.

1) 43 competent designs are categorized according to the powertrain types of their two competent modes in Table 10. As seen in that table, most of the designs consist of parallel and input-split or parallel and output-split competent mode pairs. When these designs are analyzed in detail, the competent parallel mode can be seen to meet the gradeability requirement at launch and low vehicle speed, while the competent input-split or output-split mode provides high performance at medium and high vehicle speed.
2) Although Table 10 shows a diverse set of powertrain types for competent mode pairs, only 10 designs with parallel+output-split competent mode pairs and 12 designs with parallel+input-split mode pairs can reach the 30mpg threshold. Furthermore, fully 10 of the 12 designs with parallel+input-split competent mode pairs are able to exceed 31mpg, whereas only 2 of the 10 designs with parallel+output-split com-

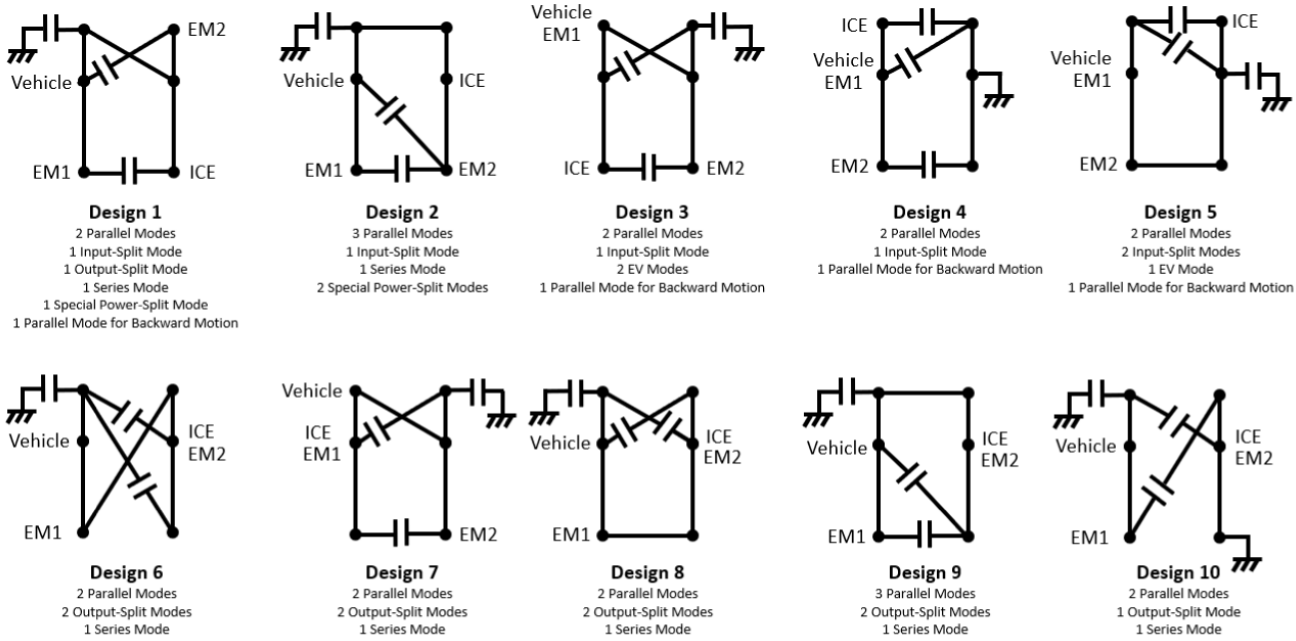

FIGURE 15. Ten competent designs with superior fuel economy.

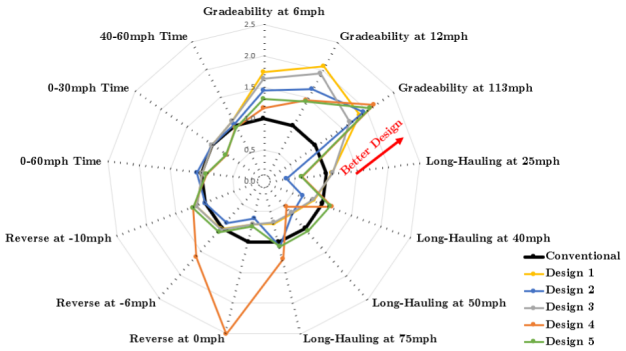

FIGURE 16. Comparison of five designs with competent parallel and input-split modes to a conventional powertrain.

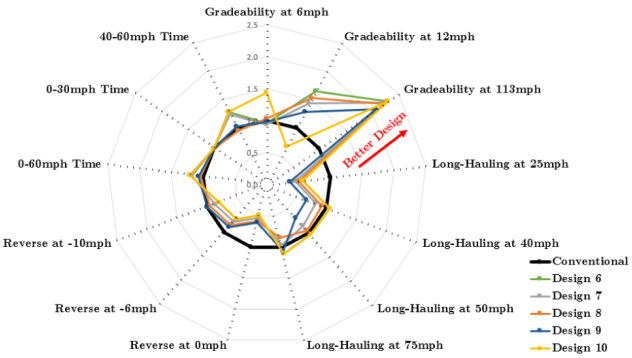

FIGURE 17. Comparison of five designs with competent parallel and output-split modes to a conventional powertrain.

petent mode pairs can exceed the same threshold. These results show that when performance and fuel economy benefits are taken into account together,

TABLE 10. 43 competent designs according to the powertrain type of competent two modes

Powertrain Types of Competent Two Modes	Number of Designs
Parallel + Output-Split	24
Parallel + Input-Split	13
Input-Split + Output-Split	1
Fixed Gear + Input-Split	1
Special Power-Split + Output-Split	1
Parallel + Compound-Split	1
Parallel + Special Power-Split	1
Fixed Gear + Parallel	1

TABLE 11. Fuel economy (F.E.) results of ten competent designs and conventional powertrain

Design No	UDDS (mpg)	HWFET (mpg)	Combined (mpg)
Conventional	19.5	26.5	22.6
Design 1	36.8	26.7	31.5
Design 2	35.7	25.3	30.1
Design 3	36.0	26.7	31.1
Design 4	35.4	26.5	30.7
Design 5	36.2	26.8	31.2
Design 6	36.5	26.7	31.4
Design 7	35.6	25.7	30.3
Design 8	35.6	25.8	30.4
Design 9	34.6	25.2	29.7
Design 10	34.7	25.3	29.8

parallel+input-split competent mode pairs have a clear superiority over parallel+output-split mode pairs.

3) When the topology of all competent output-split and input-split modes in 43 designs are investigated, input-split modes show nine unique topologies, whereas competent output-split modes show only six, although the number of competent output-split modes is higher.

Furthermore, if backward-speed capability requirements had not existed, two designs with a single input-split mode would have met all performance requirements. These results in addition to the Figs. 16-17 reveal that input-split modes are superior in terms of not only fuel economy but also performance. The observation deduced from the design process results about the superior performance of input-split modes over output-split modes is supported by the following derivations.

For an input-split powertrain type, speed equations, optimization objective for maximum acceleration, and torque constraints can be written as in (15)-(18).

$$\omega_{EM1} = f_1 \cdot \omega_{ICE} + g_1 \cdot \omega_{Vehicle} \tag{15}$$

$$\omega_{EM2} = g_2 \cdot \omega_{Vehicle} \tag{16}$$

$$minimize(T_{Vehicle}) = minimize(-g_1 \cdot T_{EM1} - g_2 \cdot T_{EM2}) \tag{17}$$

$$s.t.$$

$$T_{ICE} = -f_1 \cdot T_{EM1} \leq T_{ICEmax} \tag{18}$$

T_{EM1} and T_{EM2} can be considered the resources used to minimize the cost of $T_{Vehicle}$ within the constraints of T_{ICEmax}. As seen in these equations, T_{EM2} is a free resource since T_{EM2} can be set to $sgn(g_2) \cdot T_{EM2max}$ at a given ω_{EM2} without being restricted by T_{ICEmax}. In an input-split powertrain type, the contribution of $EM2$ to the vehicle torque is $-|g_2| \cdot T_{EM2max}$. T_{EM1} also contributes to the vehicle torque as long as $-f_1 \cdot T_{EM1} \leq T_{ICEmax}$. As a result, it is expected that an input-split powertrain type with high $|g_2|$ has superior maximum acceleration performance.

For an output-split powertrain type, speed equations, optimization objective for maximum acceleration, and torque constraints are shown in (19)-(22).

$$\omega_{EM1} = f_1 \cdot \omega_{ICE} + g_1 \cdot \omega_{Vehicle} \tag{19}$$

$$\omega_{EM2} = f_2 \cdot \omega_{ICE} \tag{20}$$

$$minimize(T_{Vehicle}) = minimize(-g_1 T_{EM1}) \tag{21}$$

$$s.t.$$

$$T_{ICE} = -f_1 \cdot T_{EM1} - f_2 \cdot T_{EM2} \leq T_{ICEmax} \tag{22}$$

As seen in these equations, T_{EM2} does not have any torque contribution to the vehicle. The only resource that can contribute to the vehicle torque is T_{EM1}. T_{EM1} may not reach its limit $sgn(g_1)T_{EM1max}$ due to the T_{ICEmax} constraint. In this case, T_{EM2} is used to relax the T_{ICEmax} constraint as $-f_1 \cdot T_{EM1} \leq T_{ICEmax} + |f_2| \cdot T_{EM2max}$. The limiting factor for minimum $T_{Vehicle}$ becomes $sgn(g_1) \cdot T_{EM1max}$ this time.

According to these derivations, an output-split powertrain type is disadvantageous in minimizing $T_{Vehicle}$ compared to an input-split powertrain type since an input-split type can use both T_{EM1} and T_{EM2} for the minimization task, whereas an output-split type has the single resource T_{EM1}.

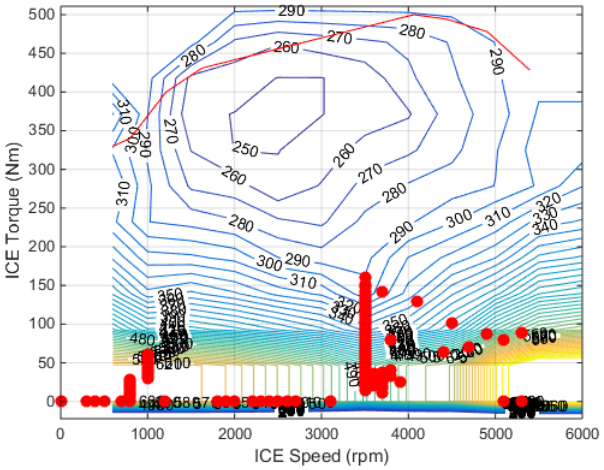

FIGURE 18. Engine operating points (red dots) of a special power-split mode during the udds drive cycle.

4) The design with a competent fixed gear powertrain type shows poor fuel economy performance since $T_{Vehicle}$ and $\omega_{Vehicle}$ determine T_{ICE} and ω_{ICE}, and no degrees of freedom exist to optimize the operating point of the engine for a drive cycle simulation.
5) Two competent modes with a special power-split powertrain type exist in the design results. However, their fuel economy cannot compete with the results of modes with input-split or output-split types. The main reason for this observation is the steady-state torque equation of a special power-split type, where $T_{Vehicle} = f_1 \cdot T_{ICE}$, while ω_{ICE} can be set independent from $\omega_{Vehicle}$. According to this equation, f_1 should be as high as possible for a superior gradeability performance. However, drive cycles used in the fuel economy simulations do not require very large $T_{Vehicle}$. Hence, T_{ICE} stays at its low range during fuel economy simulations and the degrees of freedom in ω_{ICE} are not sufficient for settling the engine at an efficient operating point. Fig. 18 shows the operating points of the engine on its fuel map as red dots, while a special power-split mode is active during the UDDS simulation. As seen in the figure, changing ω_{ICE} does not help the operating points to move to the high efficient region. This analysis shows that a high performing and fuel efficient design can be created with a competent special power-split mode if it is complemented with another fuel efficient mode.
6) Each design possesses modes with a diverse set of powertrain types ranging from EV to series, parallel, and all types of power-split. These auxiliary modes contribute to the fuel economy results, while the performance is delivered by just two competent modes in each design.
7) The effect of the PG gear ratio on performance is significant due to its presence in the coefficients of torque equations as shown in (2). Fuel economy

simulations for varying PG gear ratios reveal that a PG gear ratio can affect the fuel economy of a design between 0.2mpg and 1mpg, depending on the feasible PG ratio range. These results show that any design process that ignores PG gear ratio is incomplete. Furthermore, leveraging this result, a strategic fuel economy simulation can be conducted particularly for a large design space. In that approach, a fuel economy simulation for just one feasible PG gear ratio combination of all competent designs is first performed. 1mpg is added to the results, assuming the selected PG gear ratio gives the worst fuel economy among all combinations for a particular design. The designs with poor fuel economy results are eliminated from the design space, and fuel economy simulations for all feasible PG gear ratios of the remaining designs are conducted for benchmark. This approach saves significant computation time, since the most time-consuming task in the design process is the fuel economy simulation.

8) The most restricting design criterion is backward-speed capability when the engine is on. Previous studies have either ignored this criterion completely or looked only at the sign of the coefficient of T_{ICE} in the $\dot{\omega}_{Vehicle}$ dynamic equation. In fact, a competent design should have superior backward-speed gradeability, and the engine speed should be above its idle speed at low backward speed so that it can produce positive torque. The design process in this study takes into account all these criteria, with the result that many competent designs are eliminated because their backward-speed modes cannot meet these requirements. Only parallel modes or series modes in competent designs can meet the backward-speed capability requirement. Many designs with parallel backward-speed capable modes are eliminated because the engine speed falls below idle speed at low backward speed. If a launch clutch were added between the engine and PG node, 25 more designs would become competent.
9) Although all competent designs exceed the performance of a conventional powertrain in some respects, no competent HEV design exists that is superior in all criteria. The advantage of a conventional powertrain is the torque amplification of the torque converter at low vehicle speed.

XV. CONCLUSION

A PG-based HEV powertrain design process with systematic automated design procedures is presented in this paper. It relies on the analysis and exhaustive search of all feasible modes to generate competent HEV powertrain designs for both performance and fuel economy. The process begins with the generation of design space, which consists of all modes that can be constructed with the given set of powertrain components. Algorithms are developed to analyze the feasibility and powertrain type of each mode. After grouping the feasible modes according to their forward-speed and backward-speed capability for the engine on condition, their performance is evaluated against forward- and backward gradeability, long-hauling, acceleration time, and top speed criteria. The maximum output torque used in gradeability and acceleration time calculations is assessed through the novel problem formulation suitable to the application of linear programming techniques. The combination of modes that meets the performance requirements, along with the clutches that make the mode transitions possible, constitute the competent designs. The competent designs that include backward-speed capable modes or that can be integrated with another backward-speed capable mode are evaluated for fuel economy improvement potential using an algorithm that approximates dynamic programming optimization. The designs with superior fuel economy are depicted in the final stage.

This design process makes the following contributions to the literature. First, it shows the advantages of a mode-based design technique in the reduction of design space size and processing time. Second, not only fuel economy but also performance criteria, which are vital in vehicle design but generally ignored in earlier studies, are taken into account. Thus, the results of the process have practical value in the automotive industry. Third, computationally efficient methods are introduced to derive speed and torque equations, along with the performance characteristics of each mode. Fourth, all powertrain types that can exist in a design space with the given components are identified mathematically. This derivation mitigates the risk of omitting any design candidate in an automated process. As a result, the combination of these contributions enables the introduction of a novel exhaustive-search based design process, where PG gear ratio is also a design variable in spite of its significant effect on design space growth. Furthermore, the results of the design process show that many designs with superior fuel economy and performance can be achieved with just two PGs if the right analysis and synthesis methods are in place.

REFERENCES

[1] *Light-Duty Vehicle Greenhouse Gas Emission Standards and Corporate Average Fuel Economy Standards, Federal Register 199*, Environ. Protection Agency (EPA), Depart. Transp., Washington, DC, USA, 2012.
[2] *Motor Vehicle Safety Title 49, United States Code*, Nat. Highway Traffic Safety Admin., Washington, DC, USA, May 2013.
[3] *Performance Requirements for Determining Tow-Vehicle Gross Combination Weight Rating and Trailer Weight Rating*, SAE Standard J2807, 2012.
[4] WardsAuto Corp. *U.S. Car and Truck Sales, 1931–2016*. Accessed: Aug. 20, 2017. [Online]. Available: http://wardsauto.com/public-data
[5] K. Muta, M. Yamazaki, and J. Tokieda, "Development of new-generation hybrid system THS II—Drastic improvement of power performance and fuel economy," SAE Tech. Paper 2004-01-0064, 2004.
[6] T. M. Grewe, B. M. Conlon, and A. G. Holmes, "Defining the general motors 2-mode hybrid transmission, 2007–0273," in *Proc. Soc. Autom. Eng. World Congr.*, Detroit, MI, USA, 2007.
[7] B. Conlon *et al.*, "The next generation 'voltec' extended range EV propulsion system," *SAE Int. J. Alternative Powertrains*, vol. 4, no. 2, pp. 248–259, 2015.
[8] K. Okuda *et al.*, "Development of multi stage hybrid transmission," *SAE Int. J. Alternative Powertrains*, vol. 6, no. 1, pp. 77–83, 03 2017.

[9] J. Cobb. *December 2016 Hybrid Car Sales Numbers*. Accessed: Aug. 20, 2017. [Online]. Available: http://www.hybridcars.com/december-2016-dashboard/
[10] M. Raghavan, N. Bucknor, J. Maguire, J. Hendrickson, and T. Singh, "The design of advanced transmissions," in *Proc. FISITA World Autom. Congr.*, Yokohama, Japan, 2006.
[11] J. Liu and H. Peng, "A systematic design approach for two planetary gear split hybrid vehicles," *Veh. Syst. Dyn.*, vol. 48, no. 11, pp. 1395–1412, 2010.
[12] K. L. Cheong, P. Y. Li, and T. R. Chase, "Optimal design of power-split transmissions for hydraulic hybrid passenger vehicles," in *Proc. Amer. Control Conf.*, San Francisco, CA, USA, Jun./Jul. 2011, pp. 3295–3300.
[13] X. Zhang, H. Peng, J. Sun, and S. Li, "Automated modeling and mode screening for exhaustive search of double-planetary-gear power split hybrid powertrains," in *Proc. ASME Dyn. Syst. Control Conf.*, San Antonio, TX, USA, 2014, p. V001T15A002.
[14] M. Kang, H. Kim, and D. Kum, "Systematic configuration selection methodology of power-split hybrid electric vehicles with a single planetary gear," in *Proc. ASME Dyn. Syst. Control Conf.*, San Antonio, TX, USA, 2014, p. V001T15A001.
[15] E. Silvas, T. Hofman, A. Serebrenik, and M. Steinbuch, "Functional and cost-based automatic generator for hybrid vehicles topologies," *IEEE/ASME Trans. Mechatronics*, vol. 20, no. 4, pp. 1561–1572, Aug. 2015.
[16] X. Zhang, S. E. Li, H. Peng, and J. Sun, "Efficient exhaustive search of power-split hybrid powertrains with multiple planetary gears and clutches," *J. Dyn. Syst., Meas., Control*, vol. 137, no. 12, p. 121006, 2015.
[17] A. E. Bayrak, N. Kang, and P. Y. Papalambros, "Decomposition-based design optimization of hybrid electric powertrain architectures: Simultaneous configuration and sizing design," *J. Mech. Des.*, vol. 138, no. 7, p. 071405, 2016.
[18] W. Zhuang, X. Zhang, D. Zhao, H. Peng, and L. Wang, "Optimal design of three-planetary-gear power-split hybrid powertrains," *Int. J. Autom. Technol.*, vol. 17, no. 2, pp. 299–309, 2016.
[19] W. Zhuang, X. Zhang, H. Peng, and L. Wang, "Rapid configuration design of multiple-planetary-gear power-split hybrid powertrain via mode combination," *IEEE/ASME Trans. Mechatronics*, vol. 21, no. 6, pp. 2924–2934, Dec. 2016.
[20] S. Bai, J. Maguire, and H. Peng, *Dynamic Analysis and Control System Design of Automatic Transmissions*, 1st ed. Warrendale, PA, USA: SAE International, 2013.
[21] A. Emadi, K. Rajashekara, S. S. Williamson, and S. M. Lukic, "Topological overview of hybrid electric and fuel cell vehicular power system architectures and configurations," *IEEE Trans. Veh. Technol.*, vol. 54, no. 3, pp. 763–770, May 2005.
[22] J. M. Miller, "Hybrid electric vehicle propulsion system architectures of the e-CVT type," *IEEE Trans. Power Electron.*, vol. 21, no. 3, pp. 756–767, May 2006.
[23] C. C. Chan, A. Bouscayrol, and K. Chen, "Electric, hybrid, and fuel-cell vehicles: Architectures and modeling," *IEEE Trans. Veh. Technol.*, vol. 59, no. 2, pp. 589–598, Feb. 2010.
[24] C. Mi, A. M. Masrur, and D. W. Gao, *Hybrid Electric Vehicles: Principles and Applications With Practical Perspectives*. West Sussex, U.K.: Wiley, 2011.
[25] O. H. Dagci and H. Peng, "A method for the exploration of hybrid electric powertrain architectures with two planetary gearsets," *SAE Int. J. Alternative Powertrains*, vol. 5, no. 1, pp. 94–108, 2016.
[26] R. Mathis and Y. Rémond, "A new approach to solving the inverse problem for compound gear trains," *J. Mech. Des.*, vol. 121, no. 1, pp. 98–106, 1999.
[27] H. A. Taha, *Operations Research: An Introduction*, 9th ed. London, U.K.: Pearson, 2010.
[28] C.-C. Lin, H. Peng, J. W. Grizzle, and J.-M. Kang, "Power management strategy for a parallel hybrid electric truck," *IEEE Trans. Control Syst. Technol.*, vol. 11, no. 6, pp. 839–849, Nov. 2003.
[29] O. H. Dagci, H. Peng, and J. W. Grizzle, "Power-split hybrid electric powertrain design with two planetary gearsets for light-duty truck applications," *IFAC-PapersOnLine*, vol. 28, no. 15, pp. 8–15, 2015.
[30] G. Paganelli, S. Delprat, T. M. Guerra, J. Rimaux, and J. J. Santin, "Equivalent consumption minimization strategy for parallel hybrid powertrains," in *Proc. IEEE Veh. Technol. Conf.*, Atlantic City, NJ, USA, May 2001, pp. 2076–2081.
[31] X. Zhang, H. Peng, and J. Sun, "A near-optimal power management strategy for rapid component sizing of power split hybrid vehicles with multiple operating modes," in *Proc. Amer. Control Conf.*, Washington, DC, USA, 2013, pp. 5972–5977.

OGUZ H. DAGCI received the B.S. degree in electrical and electronic engineering from Bogaziçi University, Istanbul, Turkey, in 2000, and the M.S. degree in electrical engineering from The Ohio State University, Columbus, in 2002. He is currently pursuing the Ph.D. degree with the University of Michigan. He was a Senior Researcher with the Powertrain Control Group, General Motors Research and Development, Warren, MI, from 2002 to 2009, and a Technical Specialist with the Controls and Electronics Group, AVL Powertrain Engineering Inc., from 2011 to 2017. His current research interests are the design and control of electrified vehicles and particularly multi-mode hybrid powertrain systems.

HUEI PENG received the Ph.D. degree in mechanical engineering from the University of California at Berkeley, Berkeley, in 1992. He is currently a Professor with the Department of Mechanical Engineering, University of Michigan, Ann Arbor, MI, USA, as well as a Chang Jiang Scholar with the Tsinghua University, China. His research interests include adaptive control and optimal control, with an emphasis on their applications to vehicular and transportation systems. His current research focuses include the design and control of electrified vehicles and connected/automated vehicles. He has been an active member of the Society of Automotive Engineers (SAE) and the American Society of Mechanical Engineers. He is an SAE Fellow and an ASME Fellow.

JESSY W. GRIZZLE (S'78–M'79–SM'90–F'97) received the Ph.D. degree in electrical engineering from The University of Texas at Austin in 1983. He is a Professor in electrical engineering and computer science with the University of Michigan, Ann Arbor, MI, USA, where he holds the titles of the Elmer Gilbert Distinguished University Professor and the Jerry and Carol Levin Professor of Engineering. He is currently the Director of Michigan Robotics. He jointly holds 16 patents dealing with emissions reduction in passenger vehicles through improved control system design. He is a fellow of the IFAC. He was a recipient of the Paper of the Year Award from the IEEE Vehicular Technology Society in 1993, the George S. Axelby Award in 2002, the Control Systems Technology Award in 2003, the Bode Prize in 2012, and the IEEE TRANSACTIONS ON CONTROL SYSTEMS TECHNOLOGY Outstanding Paper Award in 2014. His work on bipedal locomotion has been the object of numerous plenary lectures and has been featured on CNN, ESPN, Discovery Channel, *The Economist, Wired Magazine, Discover Magazine, Scientific American*, and *Popular Mechanics*.